

OBSERVATIONS OF THE PROMPT GAMMA-RAY EMISSION OF GRB 070125

ERIC C. BELLM,¹ KEVIN HURLEY,¹ VALENTIN PAL'SHIN,² KAZUTAKA YAMAOKA,³ MARK S. BANDSTRA,¹
STEVEN E. BOGGS,^{1,4} SOOJING HONG,⁵ NATSUKI KODAKA,⁶ A. S. KOZYREV,⁷ M. L. LITVAK,⁷
I. G. MITROFANOV,⁷ YUJIN E. NAKAGAWA,⁸ MASANORI OHNO,⁹ KAORI ONDA,⁶
A. B. SANIN,⁷ SATOSHI SUGITA,³ MAKOTO TASHIRO,⁶ V. I. TRETYAKOV,⁷
YUJI URATA,⁶ AND CLAUDIA WIGGER¹⁰

Received 2007 November 13; accepted 2008 July 25

ABSTRACT

The long, bright gamma-ray burst GRB 070125 was localized by the Interplanetary Network. We present light curves of the prompt gamma-ray emission as observed by *Konus-Wind*, *RHESSI*, *Suzaku* WAM, and *Swift* BAT. We detail the results of joint spectral fits with *Konus* and *RHESSI* data. The burst shows moderate hard-to-soft evolution in its multi-peaked emission over a period of about 1 minute. The total burst fluence as observed by *Konus* is 1.79×10^{-4} ergs cm⁻² (20 keV–10 MeV). Using the spectroscopic redshift $z = 1.548$, we find that the burst is consistent with the “Amati” $E_{\text{peak},i}$ - E_{iso} correlation. Assuming a jet opening angle derived from broadband modeling of the burst afterglow, GRB 070125 is a significant outlier to the “Ghirlanda” $E_{\text{peak},i}$ - E_{γ} correlation. Its collimation-corrected energy release, $E_{\gamma} = 2.5 \times 10^{52}$ ergs, is the largest yet observed.

Subject heading: gamma rays: bursts

1. INTRODUCTION

The prompt gamma-ray emission of gamma-ray bursts (GRBs) is the most extensively studied aspect of these energetic explosions. Indeed, for 25 years after the discovery of GRBs (Klebesadel et al. 1973), the prompt emission was the only GRB observable available. With the first afterglow observations at longer wavelengths (Costa et al. 1997; van Paradijs et al. 1997), detailed analysis of burst models became possible. Presently, the *Swift* satellite is detecting ~ 100 bursts per year, most with rapid localization and follow-up.

The exact mechanism which produces the prompt gamma-ray emission, with its characteristic smoothly broken power-law spectrum, has not been definitively established. Recent efforts to correlate burst observables with the intrinsic burst energetics have increased the importance of detailed spectral fitting for localized bursts (for a review, see Zhang 2007). Some correlations involve the peak spectral energy E_{peak} , which is often above the ~ 150 keV cutoff of the *Swift* Burst Alert Telescope (BAT) passband.

Several current observatories are capable of detailed spectral analysis of GRBs over the full range of E_{peak} . *Konus-W* (Aptekar et al. 1995) is a double scintillator instrument on the *WIND* spacecraft. The *Ramaty High Energy Solar Spectroscopic Imager*

(*RHESSI*) is a solar observatory which uses nine germanium detectors to image the Sun at X-ray to gamma-ray energies (Lin et al. 2002). *RHESSI*'s detectors are unshielded and receive emission from astrophysical sources such as GRBs. The Wide-Band All-Sky Monitor (WAM; Yamaoka et al. 2005) aboard *Suzaku* is the large bismuth germanate (BGO) anticoincidence shield for the *Suzaku* Hard X-Ray Detector. *AGILE* (Tavani et al. 2006) and the *Gamma-Ray Large Area Space Telescope (GLAST)* (Ritz 2007) will give additional coverage at the energy range of E_{peak} and extend spectral coverage for GRBs up to tens of GeV.

In this paper, we present *Konus*, *RHESSI*, and *Suzaku* observations of the bright GRB 070125. In § 2 we discuss the observations and the localization of the burst by the Interplanetary Network (IPN). Section 3 contains the burst light curves, and in § 4 we conduct joint spectral fits to the *Konus* and *RHESSI* data.

2. OBSERVATIONS

GRB 070125 was observed by six spacecraft in the IPN: *RHESSI*, *Suzaku* WAM, and *Swift* BAT, all in low Earth orbit; the anticoincidence system of the spectrometer aboard the *International Gamma-Ray Astrophysics Laboratory (INTEGRAL)*, at 0.44 lt-s from Earth; *Konus-Wind*, at 5.4 lt-s from Earth; and the High Energy Neutron Detector and Gamma Sensor Head aboard *2001 Mars Odyssey*, at 1130 lt-s from Earth. The two other distant missions in the network, *Ulysses* and *MESSENGER* (*Mercury Surface, Space Environment, Geochemistry, and Ranging*), were off. Since *Swift* was slewing at the time of the burst, it did not immediately localize it. However, the source appeared in a routine image made after the slew was completed, and its $2.5'$ radius error circle was consistent with the initial IPN localization (Hurley et al. 2007). Even with more than 6 minutes of elapsed time since the burst onset, the BAT image detections were highly significant at 8.2σ (Racusin et al. 2007).

With only one distant spacecraft, the IPN localized the event to a long, narrow error ellipse whose area (3σ) is ~ 1200 arcmin², centered at R.A. (J2000.0) = $07^{\text{h}}51^{\text{m}}17.85^{\text{s}}$, decl. (J2000.0) = $+31^{\circ}06'12.78''$. The χ^2 for this position is 1.57 for 3 degrees of freedom. Figure 1 shows the central region of the error ellipse,

¹ UC Berkeley Space Sciences Laboratory, 7 Gauss Way, Berkeley, CA 94720-7450; ebellm@ssl.berkeley.edu.

² Ioffe Physico-Technical Institute, 26 Polytekhnicheskaya, St. Petersburg 194021, Russian Federation.

³ Department of Physics and Mathematics, Aoyama Gakuin University, 5-10-1 Fuchinobe, Sagami-hara, Kanagawa 229-8558, Japan.

⁴ Department of Physics, University of California, Berkeley, CA 94720-7300.

⁵ Laboratory of Physics, College of Science and Technology, Nihon University, 7-24-1 Narashinodai, Funabashi, Chiba 274-8501, Japan.

⁶ Department of Physics, Saitama University, 255 Shimo-Ohkubo, Sakura-ku, Saitama, Saitama 338-8570, Japan.

⁷ Institute for Space Research, Profsojuznaja 84/32, Moscow 117997, Russia.

⁸ Institute of Physical and Chemical Research (RIKEN), 2-1 Hirosawa, Wako, Saitama 351-0198, Japan.

⁹ Institute of Space and Astronautical Science, Japan Aerospace Exploration Agency (ISAS/JAXA), 3-1-1 Yoshinodai, Sagami-hara, Kanagawa 229-8510, Japan.

¹⁰ Paul Scherrer Institute, 5232 Villigen PSI, Switzerland.

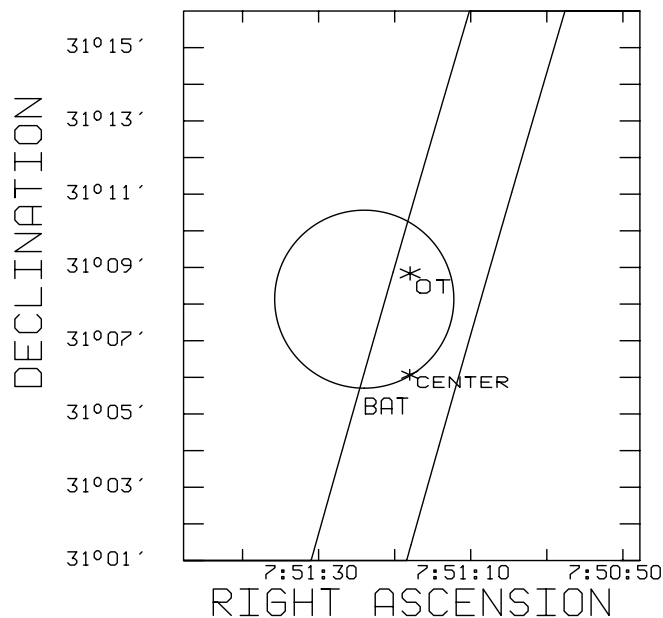


FIG. 1.—Central region of the IPN error ellipse, showing the 2.5' radius BAT 3σ error circle, the optical transient source first reported by Cenko & Fox (2007), and the center of the ellipse. The optical source lies 0.048° from the center of the IPN ellipse, on the 87% confidence contour.

with the BAT 90% confidence error circle and the optical counterpart.

Initial spectral fits to the prompt emission were reported for *RHESSI* by Bellm et al. (2007) and for *Konus* by Golenetskii et al. (2007). The initial *RHESSI* best-fit model was a cutoff power law (equivalent to the Band function below E_{break} ; see § 4) with $\alpha = 1.33_{-0.09}^{+0.11}$, $E_{\text{peak}} = 980.0 \pm 300.0$ keV, and a 30 keV–10 MeV fluence of 1.5×10^{-4} ergs cm^{-2} . The *Konus* data were best fit by a Band function with $\alpha = -1.10_{-0.09}^{+0.10}$, $\beta = -2.08_{-0.15}^{+0.10}$, and $E_{\text{peak}} = 367_{-51}^{+65}$ keV. The measured *Konus* 20 keV–10 MeV fluence was $(1.74_{-0.15}^{+0.18}) \times 10^{-4}$ ergs cm^{-2} . All errors are 90% confidence level (CL).

Pelangeon & Atteia derived a pseudo-redshift for this burst by using the *RHESSI* parameters (Pelangeon & Atteia 2007a) and the *Konus* values (Pelangeon & Atteia 2007b). These were fairly consistent at 1.6 ± 0.8 and 1.3 ± 0.3 , respectively.

Cenko & Fox (2007) reported an optical counterpart at R.A. (J2000.0) = $07^{\text{h}}51^{\text{m}}17.75^{\text{s}}$, decl. (J2000.0) = $+31^{\circ}09'04.2''$. This counterpart was confirmed by Updike et al. (2007) in the *R* band.

Racusin & Vetere (2007) reported detection by the *Swift* X-Ray Telescope (XRT). The XRT position was R.A. (J2000.0) = $7^{\text{h}}51^{\text{m}}18.08^{\text{s}}$, decl. (J2000.0) = $+31^{\circ}09'02.2''$, $4.7''$ from the optical transient reported by Cenko & Fox (2007).

Initial afterglow detections in other bands included the *Swift* UV/Optical Telescope (UVOT) in the UV (Marshall et al. 2007), radio (van der Horst 2007), and IR (Bloom et al. 2007). Milagro (Dingus 2007) observations of the source took place, but no VHE gamma-ray source was detected.

Fox et al. (2007) reported a redshift of $z \geq 1.547$ for GRB 070125 from the identification of the Mg II doublet. Cenko et al. (2008) tightened this estimate to $z = 1.5477 \pm 0.0001$. Independent observations by Prochaska et al. (2007) reported by Updike et al. (2008) reveal absorption features which are consistent with $z = 1.548$ if identified as C IV and Si IV, and the absence of Lyman absorption features requires z to be near this value.

Observations of the decaying afterglow yielded multiple possibilities for a jet break. The *Swift* XRT data showed a possible

jet break at 1.35 ± 0.35 days, but were also consistent with no jet break (Burrows & Racusin 2007; Racusin et al. 2007). Independent optical observations (Mirabal et al. 2007; Garnavich et al. 2007) showed a break in the decay at $t \geq 4$ days. The non-detection by *Chandra* (Cenko et al. 2007) was also consistent with a break occurring after 4 days. Updike et al. (2008) used a larger optical data set to fit a jet break time of $t = 3.73 \pm 0.52$ days, but cautioned that flaring made the best-fit break time dependent on the choice of time intervals. *Chandra* et al. (2008) found a best-fit break time of $t = 3.8$ days in a joint optical–X-ray fit. They suggested that the break might be chromatic, as the X-ray data alone did not require a break, and proposed that inverse Compton emission could create a delay between the optical and X-ray breaks.

Extensive observations of the afterglow of GRB 070125 allowed detailed studies of the unusual burst environment. Cenko et al. (2008) suggested that the low absorbing column densities inferred from the afterglow spectra indicate that this long burst took place in a low-density galactic halo. *Chandra* et al. (2008) performed detailed broadband fitting of the afterglow, and concluded that the immediate environment of the progenitor was likely high density ($n \sim 50 \text{ cm}^{-3}$ for a constant density profile). They also found evidence that the gamma-ray production efficiency for this burst was unusually high ($\eta_\gamma \sim 0.65$).

3. LIGHT CURVE

Figure 2 shows the *Konus*, *RHESSI*, *Suzaku* WAM, and *Swift* BAT light curves corrected for light-travel time between the spacecraft. The *Konus* trigger time was $T_{0, \text{KW}} = 07:20:50.853$. Photon travel time from *RHESSI* to *Konus* was 5.197 s, from *Suzaku* to *Konus* was 5.202 s, and from *Swift* to *Konus* was 5.215 s.

The light curves show a qualitatively similar multip peaked structure with roughly four major periods of emission. The *RHESSI* data in interval A have a slight but significant feature around $T_0 + 4$ s whose origin is unclear. The bump appears in data from all three detectors used in this study. Examination of hardness ratios suggests that the bump is softer than the rest of the emission in the interval, but insignificantly so ($\sim 1\sigma$). The difference is even more negligible when we consider only data above 65 keV. Accordingly, the bump (if extraneous) should not meaningfully influence the spectral fits reported in § 4.

T90 for the *Konus* light curve was 62.2 ± 0.8 s (20–1150 keV), for *RHESSI* 63.0 ± 1.7 s (30 keV–2 MeV), and for *Suzaku* 55 ± 2 s (50 keV–5 MeV). In the individual *Konus* bands, the T90 values were 62.8 ± 1.8 s (G1: 20–75 keV), 61.5 ± 0.9 s (G2: 75–300 keV), and 60.0 ± 5.6 s (G3: 300–1150 keV). Uncertainties on all T90 values are 1σ and were obtained by perturbing the light curves with Poisson noise and finding the new T90 values for 1000 trials. Racusin et al. (2007) report a T90 of 60 s for the *Swift* BAT light curve. Because *Swift* did not trigger on the burst, no BAT event data were stored. The available rate data contain slew artifacts; accordingly, we do not perform further analysis on the BAT data.

Both *Konus* and *RHESSI* observed the 64 ms peak flux at $T - T_0 = 41.472$ s. Using the spectral fits from § 4, the peak flux (20 keV–10 MeV) observed by *Konus* was $(1.85_{-0.36}^{+0.35}) \times 10^{-5}$ ergs $\text{cm}^{-2} \text{ s}^{-1}$. *RHESSI* observed a peak flux of $(2.92_{-0.63}^{+0.68}) \times 10^{-5}$ ergs $\text{cm}^{-2} \text{ s}^{-1}$. While the *RHESSI* fluences computed in § 4 are lower than those measured by *Konus*, *RHESSI* recorded a greater proportion of counts in the 64 ms peak interval, implying a larger peak flux. These values are moderately sensitive to background subtraction; the errors quoted are purely statistical.

Figure 3 shows the fast time evolution of hardness ratios for *Konus* and *Suzaku*. The burst shows a general softening trend in

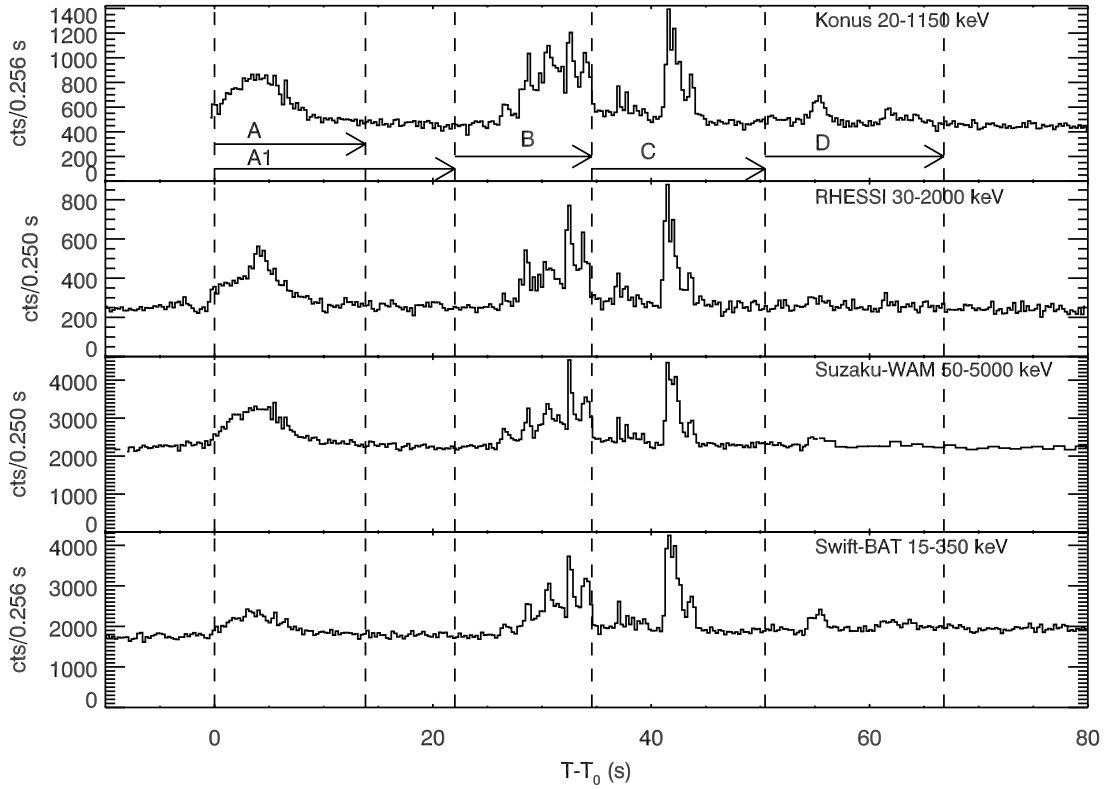


FIG. 2.—GRB 070125 light curve for *Konus*, *RHESSI* (rear segments 1, 7, and 8 only), *Suzaku* WAM, and *Swift* BAT. The light curves are adjusted for time of flight, with T_0 given in § 3. The dashed vertical lines delimit the intervals used in the time-resolved spectral fits (§ 4). The *Swift* light curve plotted contains all counts observed by *Swift*; in particular, it is not mask-tagged and therefore contains slew artifacts.

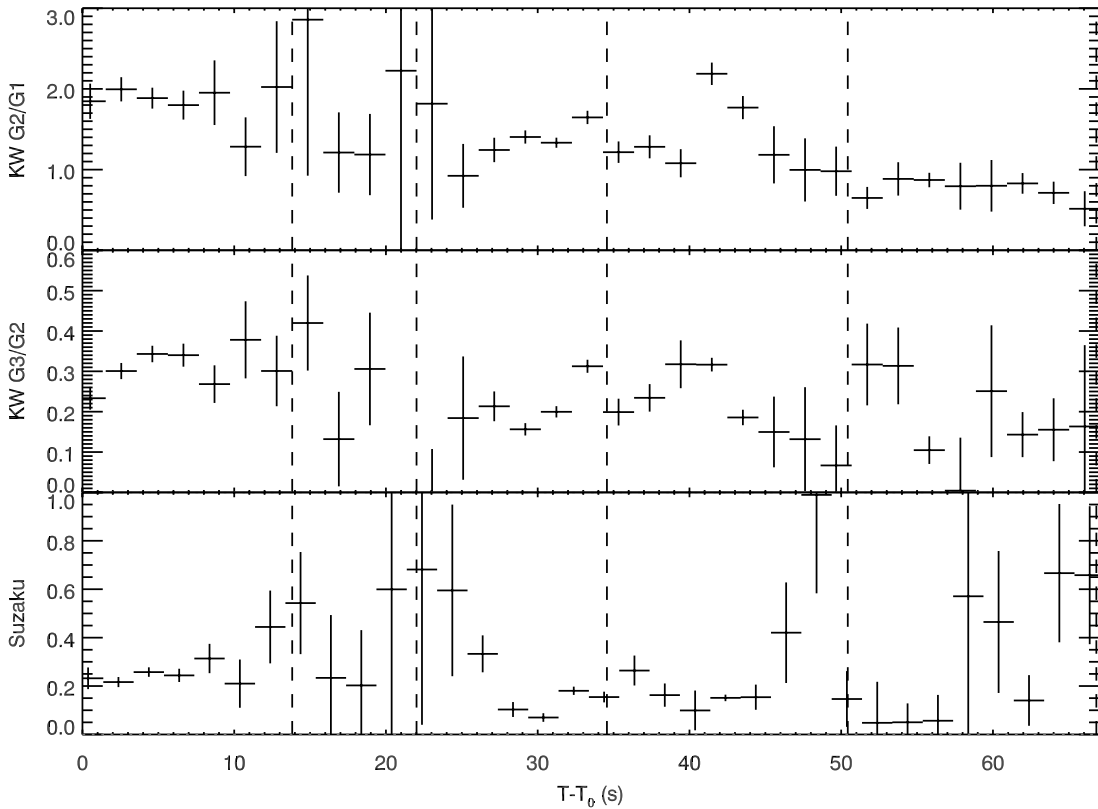


FIG. 3.—Hardness ratios for GRB 070125. The *Konus* energy bands are G1 (20–75 keV), G2 (75–300 keV), and G3 (300–1150 keV). The *Suzaku* hardness ratio plotted here is (520–5000 keV)/(50–240 keV). Dashed lines indicate spectral fitting intervals, as in Fig. 2. Points near ~ 20 s which are off-scale for the *Konus* G3/G2 ratio are consistent with zero—there is negligible emission in the G3 band at this time.

time, excepting the period of peak flux in interval C, which has comparable hardness to the initial emission in interval A.

4. SPECTRAL ANALYSIS

We performed spectral analysis for the time intervals given in Table 1 using the Konus and *RHESSI* data. While spectral data are available from *Suzaku*, the GRB photons passed through the X-Ray Spectrometer (XRS) dewar before reaching the WAM. This direction is not well calibrated for the WAM, in part due to uncertain levels of solid Ne in the dewar. With the detector response poorly understood, it is impossible to determine effectively the spectral parameters. Accordingly, we omit the *Suzaku* data in the spectral fits.

Konus 64-channel spectra are available beginning 0.512 s before the trigger and are integrated over variable timescales. The detector response, which is a function only of the burst angle relative to the instrument axis, is generated from Monte Carlo simulations described by Terekhov et al. (1998).

Because of radiation damage to the *RHESSI* detectors, only three of the nine detectors (rear segments 1, 7, and 8) were usable for this analysis. While the damaged detectors continue to record significant counts, the effect of the radiation damage on the spectral response has proven difficult to model.

To generate the *RHESSI* spectral response, we simulated monoenergetic photon beams impinging on a detailed mass model in the Monte Carlo suite MGEANT (Sturmer et al. 2000). The response of each detector changes as *RHESSI* rotates, so we used a beam geometry with photons generated along 60° arcs in rotation angle. The resulting sector responses were weighted by the burst light curve and added together. Fit results were not appreciably different when using a simple azimuthally averaged response. The beam made an angle of 165° with the *RHESSI* rotation axis to match the off-axis angle of the GRB (165.2°). The simulated photons had initial energies given by 192 logarithmically spaced bins from 10 keV to 30 MeV.

We conducted the spectral fitting in parallel using the spectral fitting packages XSPEC version 11¹¹ and ISIS version 1.4.3 (Houck 2002). The fit parameters obtained from both programs were identical. Robust fitting required a lower fit bound of 65 keV for *RHESSI*, slightly higher than the typical 30 keV lower limit. Because the GRB was arriving from the extreme rear of *RHESSI*, the photons passed through the back plate of the *RHESSI* cryostat and were hence subject to greater attenuation at low energies. The fit ranges were accordingly 20 keV–10 MeV for Konus and 65 keV–10 MeV for *RHESSI*. We rebinned the data to a minimum signal-to-noise ratio (S/N) of 2 before performing the spectral fits. This rebinning did not greatly affect the best-fit parameters. Fluence errors were obtained in ISIS by stepping through a grid of fluence values, refitting the free parameters at each grid point, and monitoring the change in χ^2 . Since it does not assume that the statistic space is quadratic, this method provides more accurate values for the uncertainties than those generated in XSPEC with the flux command.

The data were well fit in intervals A–C by a Band function (Band et al. 1993):

$$N_E = \begin{cases} A(E/E_{\text{piv}})^\alpha \exp[-E(2 + \alpha)/E_{\text{peak}}], & E < E_{\text{break}}, \\ B(E/E_{\text{piv}})^\beta, & E > E_{\text{break}}, \end{cases}$$

with $E_{\text{break}} \equiv E_{\text{peak}}[(\alpha - \beta)/(2 + \alpha)]$ and $B \equiv A\{[(\alpha - \beta)E_{\text{peak}}]/[(2 + \alpha)E_{\text{piv}}]\}^{\alpha - \beta} \exp(\beta - \alpha)$. For $\beta < -2$ and $\alpha > -2$, E_{peak}

TABLE 1
INTERVALS USED FOR SPECTRAL FITTING

| Interval | $T_i - T_0$ (s) | $T_f - T_0$ (s) | $T_f - T_i$ (s) |
|----------|--------------------|--------------------|--------------------|
| A..... | 0 | 13.824 | 13.824 |
| A1..... | 0 | 22.016 | 22.016 |
| B..... | 22.016 | 34.560 | 12.544 |
| C..... | 34.560 | 50.432 | 15.872 |
| D..... | 50.432 | 66.816 | 16.384 |
| AD..... | 0 | 66.816 | 66.816 |

NOTES.—Intervals used for spectral fitting in § 4. The reference time for Konus is $T_{0,\text{KW}} = 07:20:50.853$. For *RHESSI*, $T_{0,R} = T_{0,\text{KW}} - 5.197$ s.

corresponds to the peak of the νF_ν spectrum. The normalization A has units of photons $\text{cm}^{-2} \text{s}^{-1} \text{keV}^{-1}$, and E_{piv} is here taken to be 100 keV. For joint fits, the Band function parameters α , β , and E_{peak} were tied for both instruments, but the normalizations were allowed to vary independently. For interval D, the best-fit model after grouping was a simple power law. We report the best-fit spectral parameters in Table 2. Figure 4 shows the spectra in all intervals for the joint fit.

For single-instrument fits, the Konus data provide superior fit quality and better constraint on the fit parameters, due in part to having about 6 times more usable counts. The fit fluence, α , and β are generally consistent between *RHESSI* and Konus. However, the *RHESSI* data prefer higher E_{peak} , matching the best-fit Konus values only at the lowest end of rather large error bars. The Konus fit parameters for the total burst match well the initial values reported via the GRB Circular Network (GCN; Golenetskii et al. 2007). The *RHESSI* fit E_{peak} typically is lower here than in the value reported in the GCN (Bellm et al. 2007), but this difference is expected from fitting using the Band function rather than a cutoff power law (Band et al. 1993).

The spectral parameters for the joint fits are consistent with the Konus-only values. There are slight improvements in the uncertainties of some of the fit parameters at a cost of an increase in the χ^2 . The *RHESSI* residuals in the joint fit (Fig. 4) show a characteristic deviation pattern, indicating that the instruments disagree on the spectral shape. The Konus data dominate the fit because of their better statistical quality. The residuals for the *RHESSI*-only fits do not show any systematic deviation.

For intervals A and B, the ratio of the *RHESSI* normalization to the Konus normalization is 0.88. For interval C, the ratio is 0.95. Characteristic uncertainties for the ratio are 0.04–0.05. In interval D, the ratio for the power-law fit is $0.84^{+0.14}_{-0.13}$. Absolute normalizations in photons $\text{cm}^{-2} \text{s}^{-1} \text{keV}^{-1}$ using $E_{\text{piv}} = 100$ keV for the total interval were $(2.50^{+0.18}_{-0.15}) \times 10^{-2}$ (Konus) and $(2.25^{+0.16}_{-0.14}) \times 10^{-2}$ (*RHESSI*).

The time-resolved fits show a moderate hard-to-soft evolution; E_{peak} is largest in the initial broad pulse (539 keV) and then softens to 355 keV in interval B. The sharp pulse in interval C has a harder spectrum (418 keV). While the statistically preferred model for the S/N grouped data in interval D is a simple power law, fitting a cutoff power law with the Konus data to 2 MeV gives an estimate of E_{peak} at 220 keV. The high-energy spectral index β softens monotonically through intervals A–C.

5. ENERGETICS

Knowledge of the burst redshift $z = 1.548$ makes it possible to draw conclusions about the overall burst energetics. We assume a standard flat cold dark matter cosmology (Λ CDM), with parameters $(\Omega_\Lambda, \Omega_M, H_0) = (0.761, 0.239, 73 \text{ km s}^{-1} \text{Mpc}^{-1})$, consistent

¹¹ See <http://heasarc.gsfc.nasa.gov/docs/xanadu/xspec/>.

TABLE 2
BEST-FIT PARAMETERS FOR THE BAND FUNCTION FOR KONUS (K) AND *RHESSI* (R)

| Instruments | α | β | E_{peak} (keV) | 20 keV–10 MeV Fluence (10^{-5} ergs cm^{-2}) | χ^2/dof |
|------------------------------|-------------------------|-------------------------|----------------------------|--|---------------------|
| Total Burst (Intervals A1–D) | | | | | |
| K..... | $-1.09^{+0.09}_{-0.08}$ | $-2.09^{+0.10}_{-0.15}$ | 373^{+66}_{-51} | $17.2^{+1.5}_{-1.5}$ | 63/60 = 1.05 |
| R..... | $-0.90^{+0.46}_{-0.42}$ | $-2.24^{+0.20}_{-0.44}$ | 533^{+261}_{-171} | $16.2^{+1.7}_{-1.7}$ | 38/30 = 1.30 |
| KR..... | $-1.13^{+0.09}_{-0.08}$ | $-2.08^{+0.09}_{-0.14}$ | 430^{+80}_{-61} | $17.9^{+1.3}_{-1.3}$ $16.1^{+1.1}_{-1.1}$ | 130/93 = 1.40 |
| Interval A | | | | | |
| K..... | $-0.89^{+0.18}_{-0.15}$ | $-1.99^{+0.12}_{-0.23}$ | 447^{+154}_{-99} | $6.20^{+0.71}_{-0.75}$ | 65/61 = 1.08 |
| R..... | $-0.52^{+0.68}_{-0.42}$ | $-2.12^{+0.18}_{-0.30}$ | 512^{+249}_{-157} | $5.49^{+0.69}_{-0.71}$ | 45/32 = 1.43 |
| KR..... | $-0.96^{+0.14}_{-0.11}$ | $-2.04^{+0.12}_{-0.17}$ | 539^{+129}_{-113} | $6.22^{+0.56}_{-0.55}$ $5.48^{+0.47}_{-0.47}$ | 123/96 = 1.28 |
| Interval B | | | | | |
| K..... | $-1.07^{+0.14}_{-0.11}$ | $-2.21^{+0.14}_{-0.23}$ | 318^{+65}_{-55} | $4.88^{+0.54}_{-0.53}$ | 45/54 = 0.84 |
| R..... | $-1.12^{+0.60}_{-0.28}$ | $-2.33^{+0.30}_{-1.20}$ | 556^{+362}_{-236} | $4.82^{+0.68}_{-0.71}$ | 18/30 = 0.60 |
| KR..... | $-1.11^{+0.12}_{-0.11}$ | $-2.17^{+0.12}_{-0.20}$ | 355^{+78}_{-56} | $5.18^{+0.45}_{-0.47}$ $4.61^{+0.40}_{-0.41}$ | 76/87 = 0.88 |
| Interval C | | | | | |
| K..... | $-0.98^{+0.18}_{-0.14}$ | $-2.19^{+0.19}_{-0.54}$ | 360^{+98}_{-74} | $4.09^{+0.64}_{-0.66}$ | 44/54 = 0.82 |
| R..... | $-0.92^{+0.80}_{-0.34}$ | $-2.61^{+0.54}_{-0.54}$ | 623^{+450}_{-287} | $4.02^{+0.78}_{-0.68}$ | 30/28 = 1.08 |
| KR..... | $-1.03^{+0.16}_{-0.13}$ | $-2.19^{+0.17}_{-0.35}$ | 418^{+113}_{-84} | $4.28^{+0.54}_{-0.56}$ $4.05^{+0.50}_{-0.51}$ | 87/85 = 1.03 |
| Interval D | | | | | |
| K..... | $-1.90^{+0.07}_{-0.08}$ | | | $1.73^{+0.28}_{-0.24}$ | 32/42 = 0.77 |
| R..... | $-1.97^{+0.20}_{-0.25}$ | | | $1.34^{+0.40}_{-0.29}$ | 15/15 = 1.03 |
| KR..... | $-1.87^{+0.08}_{-0.08}$ | | | $1.84^{+0.36}_{-0.29}$ $1.48^{+0.26}_{-0.24}$ | 46/57 = 0.81 |

NOTES.—Errors are quoted at the 90% CL. For joint fits (KR), the Konus fluence is listed first. For interval D, the fit and quoted fluence are for a power-law model.

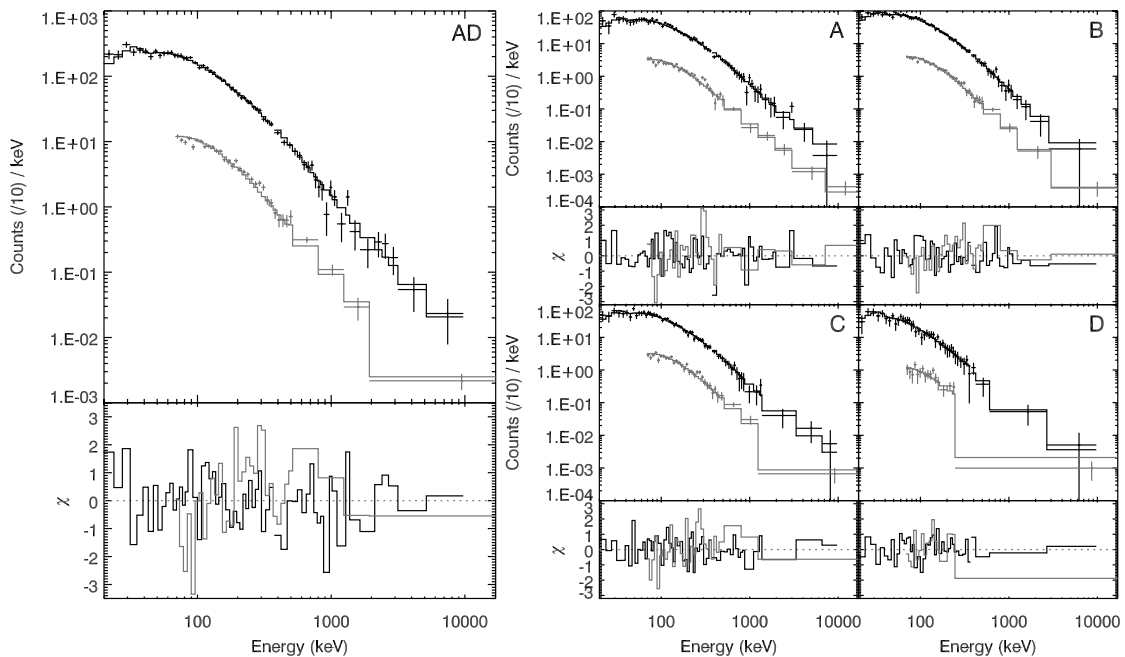


FIG. 4.—Count spectra and residuals for the joint fits. The Konus data and models are colored black, while the *RHESSI* data and models are gray. *RHESSI* data, model, and errors are divided by 10 in the count spectra plots for clarity. The overplot models differ only in normalization.

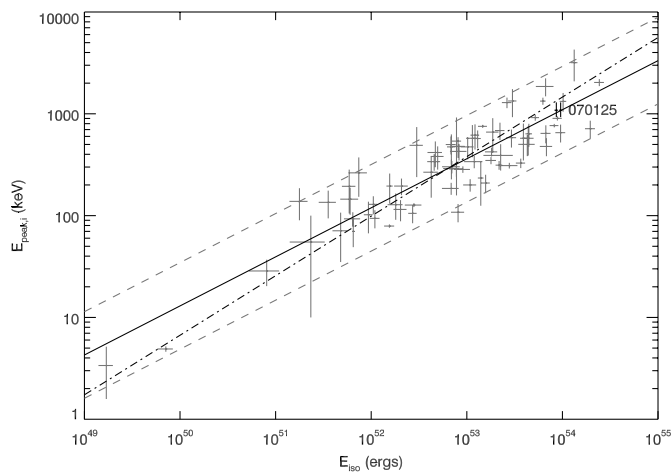


FIG. 5.—The $E_{\text{peak},i}$ - E_{iso} correlation including GRB 070125. Values of $E_{\text{peak},i}$ (the intrinsic peak energy in the burst rest frame) and E_{iso} are for the joint Konus-*RHESSI* fit. Since the normalization was allowed to vary between the two instruments, we plot separate points for Konus and *RHESSI* to indicate the corresponding values of E_{iso} . The Konus data point has the larger value of E_{iso} . Data for other bursts are from Table 1 of Ghirlanda et al. (2008), plotted using the cosmology of this paper ($\Omega_m = 0.239$, $\Omega_\Lambda = 0.761$, $h = 0.730$). The best-fit line for the unweighted data points, omitting GRB 070125, is overplot with a solid line; the 2σ scatter about that fit is indicated with dashed lines. The dash-dotted line is the best fit when the data points are weighted by their errors on both axes, again omitting GRB 070125—see text for details.

with results from *WMAP* year 3 (Spergel et al. 2007) and large-scale structure traced by luminous red galaxies (Tegmark et al. 2006). This particular set of values corresponds to the “Vanilla model” of Tegmark et al. (2006).

Extrapolating to a GRB rest-frame energy band of 1 keV–10 MeV, the isotropic emitted energy for the total burst is $(9.59 \pm 0.39) \times 10^{53}$ ergs (Konus) and $(8.67 \pm 0.38) \times 10^{53}$ ergs (*RHESSI*) for the joint fit. Because we allow independent normalizations for the Konus and *RHESSI* data, we obtain two values of E_{iso} from the joint fit, one for each instrument. The 90% CL errors are obtained by exploration of the parameter space as for the fluence; we neglect uncertainty in z . These values, together with the spectral fit of the time-integrated spectrum, are consistent with the “Amati relation” correlating E_{iso} with the intrinsic peak energy of the spectrum in the GRB rest frame $E_{\text{peak},i}$ (Amati et al. 2002; Amati 2006; Ghirlanda et al. 2008). We plot GRB 070125 in the $E_{\text{peak},i}$ - E_{iso} plane in Figure 5.

Because the best-fit Band function has a hard tail ($\beta \sim -2$), the fluence integral is sensitive to the choice of upper energy bound. If we use the observed energy band 20 keV–10 MeV, corresponding to a GRB frame band of 50 keV–25.5 MeV, the fluence is 14% larger than that in the usual bolometric band. For consistency with previous works, we will use the 1 keV–10 MeV band for bolometric estimates.

Converting the 64 ms peak fluxes reported in § 3 to bolometric peak luminosities using the best-fit Band parameters, we find peak luminosities of $(2.59^{+0.36}_{-0.37}) \times 10^{53}$ ergs s^{-1} for Konus and $(4.25^{+0.87}_{-0.79}) \times 10^{53}$ ergs s^{-1} for *RHESSI*.

Chandra et al. (2008) performed a broadband fit to afterglow data for GRB 070125. They determined a jet opening angle of $13.2^\circ \pm 0.6^\circ$ in their most plausible scenario (a radiative fireball expanding into a constant density [ISM] medium and emitting via synchrotron and inverse Compton channels). This jet angle was consistent with that inferred from the jet break time ~ 3.7 days and an emission radius derived from radio scintillation. For the

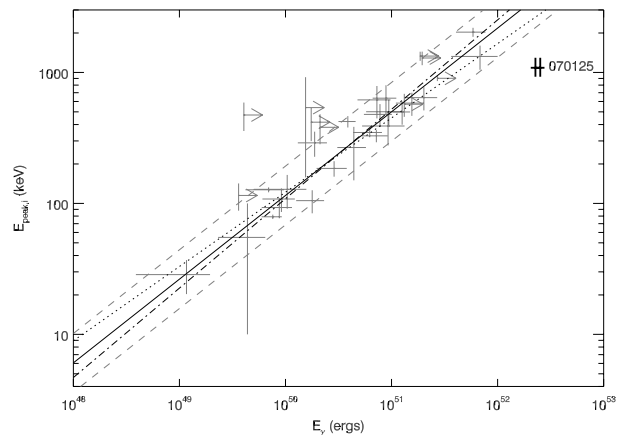


FIG. 6.—The $E_{\text{peak},i}$ - E_γ correlation including GRB 070125. Symbols and overplot fit lines same as in Fig. 5; the Konus data point has the larger value of E_γ . We also plot the best unweighted fit line including GRB 070125 with a short dotted line. Data for other bursts are from Table 1 of Ghirlanda et al. (2007), assuming an ISM density profile and plotted using the cosmology of this paper. Bursts with only lower limits on E_γ were omitted from the fit.

collimation-corrected energy $E_\gamma = (1 - \cos \theta)E_{\text{iso}}$, we find $E_\gamma = (2.52 \pm 0.24, 2.27 \pm 0.22) \times 10^{52}$ ergs for (Konus, *RHESSI*). These values are the largest yet recorded for a burst with measured E_{peak} (cf. Frail et al. 2006; Kocevski & Butler [2008] also reported lower limits on E_γ greater than 10^{52} ergs for several *Swift* bursts using the time of the last XRT observation). We plot GRB 070125 in the $E_{\text{peak},i}$ - E_γ plane in Figure 6 to examine its consistency with the “Ghirlanda” $E_{\text{peak},i}$ - E_γ correlation (Ghirlanda et al. 2004, 2007).

In Figures 5 and 6 we also overplot the best-fit correlation lines. A number of fitting approaches have been considered in the literature in an effort to account for the apparent extrastatistical spread of the points about the correlation (for a review, see Ghirlanda et al. 2008). We have followed Ghirlanda et al. (2008) in presenting two least-squares fits, one in which the data points are unweighted and a second in which the errors on both axes are considered. After the fit, we estimate the dispersion of the points perpendicular to the best-fit correlation line using the square root of the bias-corrected sample variance.

GRB 070125 is quite consistent with the Amati relation: including it in the fit makes negligible changes in the best-fit correlation slope or the logarithmic dispersion (0.20 dex). However, it is a 5.0σ outlier to the Ghirlanda correlation fitted without it, using the sample dispersion to estimate σ . Including GRB 070125 in an unweighted fit of the bursts in the Ghirlanda sample, the overall dispersion increases to 0.13 dex (from 0.09 dex), and GRB 070125 remains a 2.8σ outlier.

The unusual environment of GRB 070125 is responsible for its high value of E_γ . In particular, the jet opening angle of $13.2^\circ \pm 0.6^\circ$ derived by Chandra et al. (2008) is larger than all of those presented by Ghirlanda et al. (2007). Retaining the 3.7 ± 0.5 day jet break time well established in the optical (Updike et al. 2008; Chandra et al. 2008), we may derive the jet opening angle assuming adiabatic emission and more conventional parameters (Sari et al. 1999). Assuming an interstellar medium (ISM) profile with circumburst density $n = 3 \text{ cm}^{-3}$ and a gamma-ray production efficiency of $\eta_\gamma = 0.2$, the corresponding jet opening angle is $\theta = 5.6^\circ \pm 0.3^\circ$ for Konus. The resulting collimation-corrected energy would be $E_\gamma = (4.6 \pm 0.5) \times 10^{51}$ ergs, only 0.8σ from the best-fit correlation omitting GRB 070125.

6. DISCUSSION

While GRB 070125 had a large measured prompt gamma-ray fluence, its spectral properties are unremarkable. The values of the best-fit spectral parameters are similar to those observed for other bright bursts (e.g., Kaneko et al. 2006), and the spectral evolution observed is similarly common. The environment of GRB 070125 is unique, however (Cenko et al. 2008; Chandra et al. 2008; Utdike et al. 2008), requiring a broad jet opening angle in broadband afterglow models (Chandra et al. 2008). After collimation correction, GRB 070125 has the most energetic prompt emission yet observed and is a significant outlier to the correlation between peak energy and E_γ .

GRB 070125 appears to weaken the claim that the Ghirlanda correlation has low dispersion. GRB 070125 is not a “recognizable” outlier to the Ghirlanda relation in the sense of Ghirlanda et al. (2007), as it is highly consistent with the Amati relation. Its jet parameters have been derived from a rich and well-sampled afterglow data set. While the circumburst environment of this GRB is unusually dense, this only highlights the assumption of a fairly narrow range of efficiency and density parameters for the majority of GRBs where broadband modeling of the afterglow has not been possible. The true dispersion of the correlation may in fact be larger.

The physical significance of GRB spectrum-energy correlations has been questioned (e.g., Butler et al. 2007, 2008). In particular, detector trigger thresholds affect burst detection, and more complex selection effects govern the measurement of peak energies, redshifts, and afterglow breaks. These effects can influence the sample of GRBs with known redshift, $E_{\text{peak},i}$, and E_γ . Ghirlanda et al. (2008) examined the effect of trigger and spectral analysis thresholds in the E_{peak} -fluence plane, finding that the *Swift*-detected burst sample was truncated by the spectral analysis threshold. Neither threshold truncated the pre-*Swift* burst sample.

We were unable to confirm the source of the systematic shift in E_{peak} and fluence between the two instruments for this burst. Minor radiation damage was becoming noticeable in *RHESSI* detector 8 near the time of this work, mostly below the 65 keV cut utilized here. It is also possible that the Monte Carlo simulation of the *RHESSI* response is less accurate for such extreme off-axis angles, where a greater number of interactions with the cryostat may be expected.

Our previous work had found excellent agreement in all fit parameters for independent *RHESSI* and Konus spectral fits for GRB

051103 and GRB 050717. For the short GRB 051103, Konus found $E_{\text{peak}} = 1920 \pm 400$ keV and a 20 keV–10 MeV fluence of $4.4 \pm 0.5 \times 10^{-5}$ ergs cm^{-2} (Golenetskii et al. 2005; Frederiks et al. 2007). A *RHESSI* fit yielded $E_{\text{peak}} = 1930 \pm 340$ keV and 20 keV–10 MeV fluence of 4.5×10^{-5} ergs cm^{-2} (Bellm et al. 2006). Krimm et al. (2006) found for a cutoff power-law fit to Konus data for GRB 050717 a best-fit value of $E_{\text{peak}} = 2101_{-830}^{+1934}$ keV. A *RHESSI* fit to the same burst found $E_{\text{peak}} = 1550_{-370}^{+510}$ keV (Wigger et al. 2006). Those bursts had *RHESSI* off-axis angles of 97° and 110° , respectively.

Joint spectral fits to *Swift* BAT and *RHESSI* data for 25 bursts co-observed by the two instruments between 2004 December and 2006 December indicated that no offset in response normalization was needed for the two instruments (Bellm et al. 2008). However, for two of three bursts occurring during or after 2006 December, the *RHESSI* data showed a significant deficit relative to *Swift* BAT. The *RHESSI* polar angles for all three late bursts were between 90° and 110° . These fits were conducted using only detectors 1 and 7, which do not appear to have radiation damage in background spectra during this interval. Nonetheless, these results suggest that the observed offset in the *RHESSI* and Konus fit parameters found here is more likely a consequence of increased radiation damage in the *RHESSI* detectors than a geometric effect or a generic offset in the *RHESSI* simulations.

Future analysis of archival bursts may help identify the source of any systematic effects present here. It is clear, however, that joint fits between instruments capable of constraining the full range of E_{peak} are valuable in providing the most accurate and precise determination of the fit parameters.

This work was supported by *Swift* AO-2 GI grant NNG06GH58G, “Completing *Swift* GRB Energy Spectra with Konus and *RHESSI*” and by the AO-3 grant NNX07AE86G. K. H. is grateful for IPN support under JPL Contract 1282043, and NASA grants NNG06GI896, NNX06AI36G, NNG06GE69G, and NAG5-13080. The Konus-*Wind* experiment is supported by a Russian Space Agency contract and RFBR grant 06-02-16070. We thank Bob Lin, David Smith, and Dieter Hartmann for helpful comments.

Facilities: RHESSI, WIND (Konus)

REFERENCES

- Amati, L. 2006, *MNRAS*, 372, 233
 Amati, L., et al. 2002, *A&A*, 390, 81
 Aptekar, R. L., et al. 1995, *Space Sci. Rev.*, 71, 265
 Band, D., et al. 1993, *ApJ*, 413, 281
 Bellm, E., Bandstra, M. E., Boggs, S. E., Hurley, K., Wigger, C., Hajdas, W., & Smith, D. M. 2006, *BAAS*, 9, 13.05
 Bellm, E., Bandstra, M., Boggs, S., Wigger, C., Hajdas, W., Smith, D. M., & Hurley, K. 2007, *GCN Circ.* 6025, <http://gcn.gsfc.nasa.gov/gcn/gcn3/6025.gcn3>
 Bellm, E. C., Bandstra, M. E., Boggs, S. E., Hajdas, W., Hurley, K., Smith, D. M., & Wigger, C. 2008, in *AIP Conf. Proc.* 1000, *Gamma-Ray Bursts 2007*, ed. M. Galassi, D. Palmer, & E. Fenimore (New York: AIP), 154
 Bloom, J. S., Starr, D., & Blake, C. H. 2007, *GCN Circ.* 6054, <http://gcn.gsfc.nasa.gov/gcn/gcn3/6054.gcn3>
 Burrows, D. N., & Racusin, J. 2007, *GCN Circ.* 6181, <http://gcn.gsfc.nasa.gov/gcn/gcn3/6181.gcn3>
 Butler, N. R., Kocevski, D., & Bloom, J. S. 2008, *ApJ*, submitted (arXiv:0802.3396v1)
 Butler, N. R., Kocevski, D., Bloom, J. S., & Curtis, J. L. 2007, *ApJ*, 671, 656
 Cenko, S. B., & Fox, D. B. 2007, *GCN Circ.* 6028, <http://gcn.gsfc.nasa.gov/gcn/gcn3/6028.gcn3>
 Cenko, S. B., Soderberg, A. M., Frail, D. A., & Fox, D. B. 2007, *GCN Circ.* 6186, <http://gcn.gsfc.nasa.gov/gcn/gcn3/6186.gcn3>
 Cenko, S. B., et al. 2008, *ApJ*, 677, 441
 Chandra, P., et al. 2008, *ApJ*, 683, 924
 Costa, E., et al. 1997, *Nature*, 387, 783
 Dingus, B. 2007, *GCN Circ.* 6026, <http://gcn.gsfc.nasa.gov/gcn/gcn3/6026.gcn3>
 Fox, D. B., Berger, E., Price, P. A., & Cenko, S. B. 2007, *GCN Circ.* 6071, <http://gcn.gsfc.nasa.gov/gcn/gcn3/6071.gcn3>
 Frail, D. A., et al. 2006, *ApJ*, 646, L99
 Frederiks, D. D., Palshin, V. D., Aptekar, R. L., Golenetskii, S. V., Cline, T. L., & Mazets, E. P. 2007, *Astron. Lett.*, 33, 19
 Garnavich, P., et al. 2007, *GCN Circ.* 6165, <http://gcn.gsfc.nasa.gov/gcn/gcn3/6165.gcn3>
 Ghirlanda, G., Ghisellini, G., & Lazzati, D. 2004, *ApJ*, 616, 331
 Ghirlanda, G., Nava, L., Ghisellini, G., & Firmani, C. 2007, *A&A*, 466, 127
 Ghirlanda, G., Nava, L., Ghisellini, G., Firmani, C., & Cabrera, J. I. 2008, *MNRAS*, 387, 319
 Golenetskii, S., Aptekar, R., Mazets, E., Pal’Shin, V., Frederiks, D., & Cline, T. 2007, *GCN Circ.* 6049, <http://gcn.gsfc.nasa.gov/gcn/gcn3/6049.gcn3>
 Golenetskii, S., et al. 2005, *GCN Circ.* 4197, <http://gcn.gsfc.nasa.gov/gcn/gcn3/4197.gcn3>
 Houck, J. C. 2002, in *High Resolution X-Ray Spectroscopy with XMM-Newton and Chandra*, ed. G. Branduardi-Raymont (London: MSSL), 17
 Hurley, K., et al. 2007, *GCN Circ.* 6024, <http://gcn.gsfc.nasa.gov/gcn/gcn3/6024.gcn3>

- Kaneko, Y., Preece, R. D., Briggs, M. S., Paciasas, W. S., Meegan, C. A., & Band, D. L. 2006, *ApJS*, 166, 298
- Klebesadel, R. W., Strong, I. B., & Olson, R. A. 1973, *ApJ*, 182, L85
- Kocevski, D., & Butler, N. 2008, *ApJ*, 680, 531
- Krimm, H. A., et al. 2006, *ApJ*, 648, 1117
- Lin, R. P., et al. 2002, *Sol. Phys.*, 210, 3
- Marshall, F. E., vanden Berk, D. E., & Racusin, J. 2007, *GCN Circ.* 6041, <http://gcn.gsfc.nasa.gov/gcn/gcn3/6041.gcn3>
- Mirabal, N., Halpern, J., & Thorstensen, J. R. 2007, *GCN Circ.* 6096, <http://gcn.gsfc.nasa.gov/gcn/gcn3/6096.gcn3>
- Pelangeon, A., & Atteia, J.-L. 2007a, *GCN Circ.* 6033, <http://gcn.gsfc.nasa.gov/gcn/gcn3/6033.gcn3>
- . 2007b, *GCN Circ.* 6059, <http://gcn.gsfc.nasa.gov/gcn/gcn3/6059.gcn3>
- Prochaska, J. X., Roelofs, G., Bloom, J., & Steeghs, D. 2007, *GCN Circ.* 6032, <http://gcn.gsfc.nasa.gov/gcn/gcn3/6032.gcn3>
- Racusin, J. L., Cummings, J., Marshall, F. E., Burrows, D. N., Krimm, H., & Sato, G. 2007, *GCN Rep.*, 28, 3
- Racusin, J., & Vetere, L. 2007, *GCN Circ.* 6030, <http://gcn.gsfc.nasa.gov/gcn/gcn3/6030.gcn3>
- Ritz, S. 2007, in *AIP Conf. Proc.* 921, *The First GLAST Symposium*, ed. S. Ritz, P. Michelson, & C. A. Meegan (New York: AIP), 3
- Sari, R., Piran, T., & Halpern, J. P. 1999, *ApJ*, 519, L17
- Spergel, D. N., et al. 2007, *ApJS*, 170, 377
- Sturmer, S. J., Seifert, H., Shrader, C., & Teegarden, B. J. 2000, in *AIP Conf. Proc.* 510, *The Fifth Compton Symposium*, ed. M. L. McConnell & J. M. Ryan (New York: AIP), 814
- Tavani, M., et al. 2006, *Proc. SPIE*, 6266, 626603
- Tegmark, M., et al. 2006, *Phys. Rev. D*, 74, 123507
- Terekhov, M. M., Aptekar, R. L., Frederiks, D. D., Golenetskii, S. V., Il'Inskii, V. N., & Mazets, E. P. 1998, in *AIP Conf. Proc.* 428, *Gamma-Ray Bursts: 4th Huntsville Symposium*, ed. C. A. Meegan, R. D. Preece, & T. M. Koshut (New York: AIP), 894
- Urdike, A. C., Hartmann, D. H., Bryngelson, G. L., Goldthwaite, R. C., & Puls, J. R. 2007, *GCN Circ.* 6029, <http://gcn.gsfc.nasa.gov/gcn/gcn3/6029.gcn3>
- Urdike, A. C., et al. 2008, *ApJ*, 685, 361
- van der Horst, A. J. 2007, *GCN Circ.* 6042, <http://gcn.gsfc.nasa.gov/gcn/gcn3/6042.gcn3>
- van Paradijs, J., et al. 1997, *Nature*, 386, 686
- Wigger, C., Hajdas, W., Zehnder, A., Hurley, K., Bellm, E., Boggs, S., Bandstra, M., & Smith, D. M. 2006, *Nuovo Cimento B*, 10, 1117
- Yamaoka, K., et al. 2005, *IEEE Trans. Nucl. Sci.*, 52, 2765
- Zhang, B. 2007, *Chinese J. Astron. Astrophys.*, 7, 1